Technology and Health Care 23 (2015) S231–S238
DOI 10.3233/THC-150958
IOS Press

BP neural network tuned PID controller for position tracking of a pneumatic artificial muscle

Jizhuang Fan, Jun Zhong, Jie Zhao and Yanhe Zhu*
State Key Laboratory of Robotics Institute, Harbin Institute of Technology University, Harbin, Heilongjiang, China

Abstract.
BACKGROUND: Although Pneumatic Artificial Muscle (PAM) has a promising future in rehabilitation robots, it's difficult to realize accurate position control due to its highly nonlinear properties.
OBJECTIVE: This paper deals with position control of PAM.
METHODS: To describe the hysteresis inside PAM, a polynomial based phenomenological function is developed. Based on the phenomenological model for PAM and analysis of pressure dynamics within PAM, an adaptive cascade controller is proposed. Both outer loop and inner loop employ BP Neural Network tuned PID algorithm. The outer loop is to handle high nonlinearities and unmodeled dynamics of PAM, while the inner loop is responsible for nonlinearities caused by pressure dynamics.
RESULTS: Experimental results show high tracking accuracy as compared with a convention PID controller.
CONCLUSION: The proposed controller is effective in improving performance of PAM and will be implemented in a rehabilitation robot.

Keywords: Mckibben muscles, empirical modeling, BP neural network tuned PID, cascade position controller

1. Introduction

Rehabilitation robots have been studied in recently years [1–4]. As a flexible actuator, pneumatic artificial muscle (PAM) has been widely used in medical robots [3,4]. However, strong hysteresis exists within PAM. To overcome challenges produced by inherent hysteresis of PAM, many models have been proposed [5–15]. The most widely spread model [7], was derivated from assumed geometric features and principle of virtual work. Later scientists proposed enhanced models by including several important geometric feaures of PAM [8–13]. Several other phenomenological behavior models of PAM were developed by later researchers [14,15].

Based on respective analytic models, different control algorithms have been applied in position control. Adaptive pole-placement scheme [16], gain scheduling approach [17], and sliding-mode algorithm [18] were used in the position control system actuated by PAMs. Combination of controlling algorithms were also adopted in position control scheme of PAMs [19–21].

*Corresponding author: Yanhe Zhu, State Key Laboratory of Robotics Institute, Harbin Institute of Technology University, Room 203, Building C1, Science Square, Yikuang Street No. 2, Nangang District, Harbin 150006, Heilongjiang, China. Tel.: +86 13074594165; Fax: +86 0451 86414538; E-mail: yhzhu@hit.edu.cn

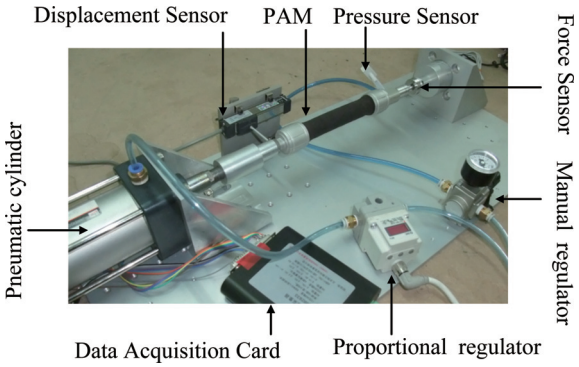

Fig. 1. Experimental set-up for modeling PAM.

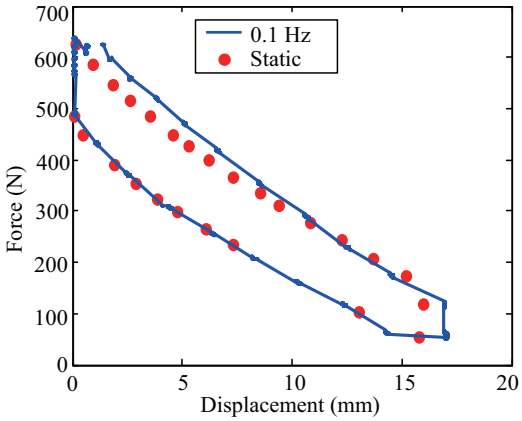

Fig. 2. Quasi rate-independent characteristic of PAM.

A cascade controller is proposed in this paper, whose inner loop deals with controlling pressure dynamics and the outer loop is used in position tracking. This cascade structure can reduce the effort in handling nonlinearities and unmodeled dynamics by only single loop. Conventional PID controller cannot work on the single-input/multi-output systems with high nonlinear and time varying properties because the classic PID shows inflexibility on uncertain factors such as unmodeled dynamics, modeling errors, time varying characteristics and external disturbances. To solve this challenging task, an optional choice is to tune controller parameters online according to real time feedback information. By ceaselessly changing controller parameters, uncertain factors can be handled and performance would be improved. With great capacity in adaptive, parallel and fault tolerance, BP Neural Network (NN) is adopted in tuning parameters of PID controller online on the basis of feedback signals.

In this paper, Section 2 derives a phenomenological model depicting force-displacement-pressure relationship of PAM. Structure of 1-DOF manipulator actuated by PAM is introduced in Section 3. An adaptive cascade PID controller is proposed for this manipulator. Experiments are performed to verify the control scheme in Section 4. Conclusion is done in Section 5.

2. Empirical model of PAM

2.1. Description of the set-up

Experimental set-up for modeling PAM is displayed in Fig. 1. Three type information – pressure inside PAM (DMSP-20-120RMCM, FESTO Corporation), contractile force and corresponding displacement – are sampled in real time. To obtain experimental data, predetermined pressure is applied to PAM by manual regulator and the accurate value of pressure inside PAM is measured by the pressure sensor. Pressure with low frequencies is applied to cylinder. Corresponding sampled pressure, force and displacement are filtered and then used to build up a model of PAM.

2.2. PAM model building up and validation

Researchers pointed out that hysteresis inside PAM is quasi rate-independent [7,15]. In this research, this property is tested. The experimental curves are plotted in Fig. 2, where two loops of different frequency are compared. The static hysteretic curve is acquired in the following way: increases the pressure

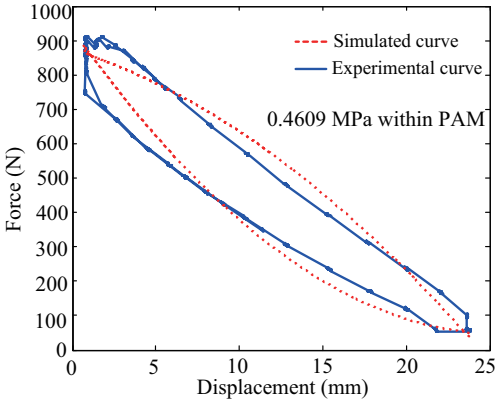

Fig. 3. Validation of the proposed polynomial model.

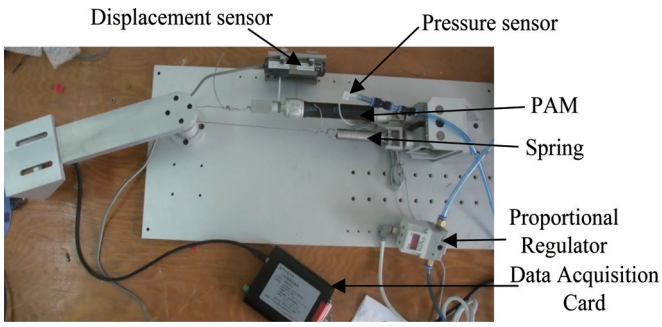

Fig. 4. 1-DOF experimental set-up actuated by PAM.

inside pneumatic cylinder very slowly (0.001 Hz) while constant pressure is applied to PAM. The 0.1 Hz hysteretic loop is acquired when pressure within PAM is at a constant value of 0.3 MPa and pressure of sinusoidal wave with frequency 0.1 Hz is applied to pneumatic cylinder. This weak rate-dependent characteristic is the basis of the empirical model of PAM. This closed loop could be depicted by following equation:

$$F = ax^2 + bx + c + (dx^2 + ex + f)sign(dx/dt) \tag{1}$$

Where F symbols the contractile force, x is corresponding displacement and a, b, c, d, e, f determine curve shape. These five parameters are optimized using least squares curve fitting method based on experimental data. The component, $(dx^2 + ex + f)sign(dx/dt)$, represents the hysteretic value of contractile force between shortening and lengthening process.

Based on hysteretic curves, parameters in Eq. (1) are optimized by least square method. Different pressures within PAM mean different hysteretic curves and different optimal values of these five parameters, a, b, c, d, e, f. These different values are carefully addressed with respect to pressure values inside PAM. Relationships between parameters and pressures are fitted by five quadratic polynomial equations as follows:

$$\begin{aligned} a &= -1.094 * p^2 - 0.9724 * p + 0.9316, \quad b = -20.81 * p^2 + 3.49 * p - 39.31 \\ c &= -1018 * p^2 + 2732 * p - 139.6, \quad d = 2.752 * p^2 - 4.697 * p + 2.664 \\ e &= -103.6 * p^2 + 139.6 * p - 69.04, \quad f = -251.6 * p^2 + 167.4 * p + 5.416 \end{aligned} \tag{2}$$

To validate the proposed model, pressure in the form $pressure = 0.16 \sin(0.2\pi t) + 0.16$ are applied to pneumatic cylinder when PAM is at pressure of 0.4609 MPa. The predicted result and experimental curve are plotted in Fig. 3 and comparison between the two curves indicates that the model has good capacity in capturing hysteresis within PAM.

3. Cascade position controller design for PAM

Figure 4 displays a manipulator actuated by PAM. PAM in the manipulator provides rotary torque. Passive spring provides resilient force when link comes back to balancing position. To realize position

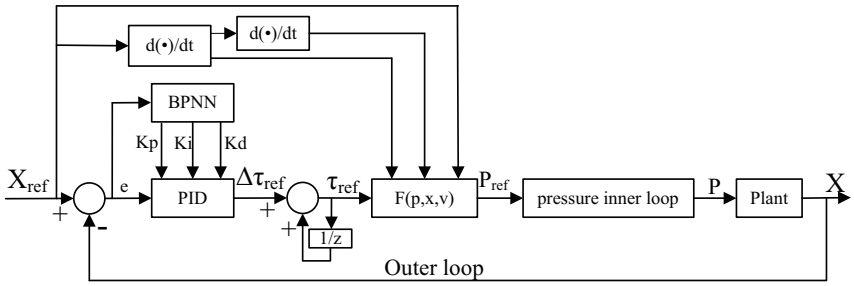

Fig. 5. The structure of the cascade position controller for the manipulator.

control of PAM, what should be done is to change voltage input for regulator. Obviously, the only controllable variable is the voltage command produced by Data Acquisition Card. The load dynamics is presented as follow

$$\tau = (f - kr\theta)r = J\ddot{\theta} \tag{3}$$

Where τ [N $\cdot$ cm] is the resultant torque, J is rotary inertia, f [N] symbols tension of PAM, k [N/m] is resilience factor of spring, r [m] is rotating radius, and θ [rad] is angular rotation.

The structure of the designed controller is depicted in Fig. 5. Incorporating Eqs (1) to (3) to the cascade control scheme, inner loop is responsible for pressure dynamics and outer loop deals with tracking position. BP Neural Network algorithm is integrated to the outer and inner loop of the scheme.

3.1. Outer loop for position control and inner loop for pressure dynamics

Figure 5 shows that outer loop provides the reference torque τ_{ref}. Then τ_{ref} is used to calculate the required pressure p_{ref} by the function $F(p, x, v)$ that is derived from aforementioned equations. p_{ref} is the input of inner pressure loop. Parameters (k_p, k_i, k_d) for the outer loop are key factors affecting the controller's performance. In this paper, these three parameters are tuned on-line using BP Neural Network.

Pressure dynamics eaquations can be derivated from fluid mechanics equations. However, it's difficult to establish accurate equations because volume of PAM and parameters of regulator can't be accurately acquired. In this research, a nonparametric BPNN tuned PID controller is adopted to cope with pressure control within PAM. The schematic is shown in Fig. 6.

3.2. BP neural network structure for online tuning PID parameters

A BP neural network containing three layers is illustrated in Fig. 7. From left to right, these three layers have three input nodes, four hidden nodes, and three output nodes, respectively. The inputs of BPNN are related to the error between desired value and sampled value in the following ways

$$x_1(n) = X_{ref}(n), \quad x_2(n) = X_{sampled}(n), \quad x_3(n) = X_{ref}(n) - X_{sampled}(n) \tag{4}$$

If proper $k_p\,(0)$, $k_i\,(0)$, $k_d\,(0)$ are selected, the tuned parameters after per tuning operation are modified as follows

$$k_p(n) = k_p(n-1) + \Delta k_p(n), \quad k_i(n) = k_i(n-1) + \Delta k_i(n), \quad k_d(n) = k_d(n-1) + \Delta k_d(n) \tag{5}$$

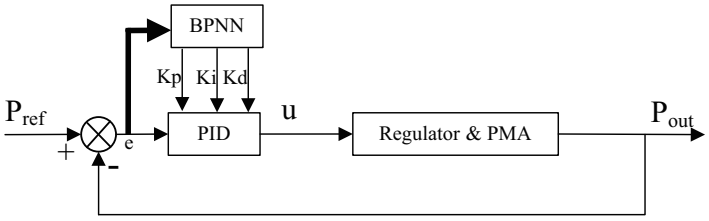

Fig. 6. Inner loop control for pressure dynamics.

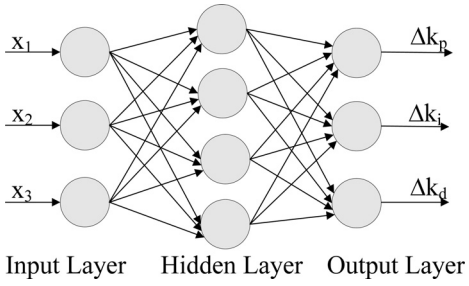

Fig. 7. BP neural network for online tuning PID parameters.

In order to minimize errors between input commands and sampled values, weights of BPNN should be adjusted online according to some criteria. In this paper, a cost function is defined in Eq. (6) to provide the criteria

$$J(n) = \frac{1}{2}\left(X_{ref}(n) - X(n)\right)^2 \tag{6}$$

Without loss of generality, the rules of updating weights are obtained in the direction of gradient descent and defined in Eqs 7(a) and (b) for hidden layer and output layer, respectively

$$\Delta w_{ij}^{(2)}(n) = -\eta \frac{\partial J(n)}{\partial w_{ij}^{(2)}(n)} + \alpha \Delta w_{ij}^{(2)}(n-1) \tag{7a}$$

$$\Delta w_{ij}^{(3)}(n) = -\eta \frac{\partial J(n)}{\partial w_{ij}^{(3)}(n)} + \alpha \Delta w_{ij}^{(3)}(n-1) \tag{7b}$$

Where η is learning rate and α the inertia factor, $w_{ij}^{(2)}$ (i = 1, 2, 3, j = 1, 2, 3, 4) is defined as the influencing weight of output from ith node in first layer on input of jth node of second layer. $w_{ij}^{(3)}$ (i = 1, 2, 3, 4, j = 1, 2, 3) measures the influence of output from ith node in second layer on input of jth node in third layer. More details are described in [22].

4. Experimental results and discussion

Experiments are conducted at different wave excitations for purpose of validating the capacity of the controller. Figure 8(a) shows the position responses to step inputs under 0.2 Hz and amplitude 10 mm. To better perform the validation of the proposed controller, performance from conventional PID cascade position controller is also drawn in Fig. 8(a). Observing response curves from conventional PID controller, a 10% overshoot happens in the tracking curves of conventional PID controller and oscillations are obvious in transient response to rising input command. From curves of BPNN-PID position controller, the maximum overshoot is obviously smaller than overshoot from conventional PID position curves. At descending stages in square excitation, responses of BPNNPID controller are faster than responses of classic PID controller, which could be observed in time intervals [2.5, 4] (s) and [7.5, 9] (s). Figure 8(b) displays position responses to square wave input of 0.1 Hz with amplitude 20 mm, which also demonstrates better performance of BPNNPID than performance of classic PID. Sinusoid wave excitations of

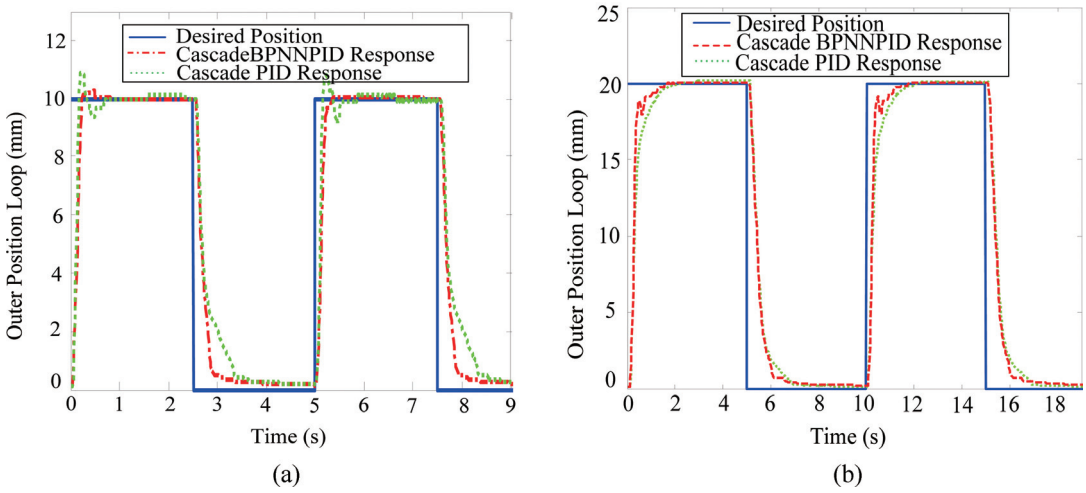

Fig. 8. Comparison between performance of cascade BPNNPID scheme and performance of conventional cascade PID scheme: (a) step responses to the step input with 0.2 Hz and amplitude 10 mm; (b) step responses to the step input with 0.1 Hz and amplitude 20 mm.

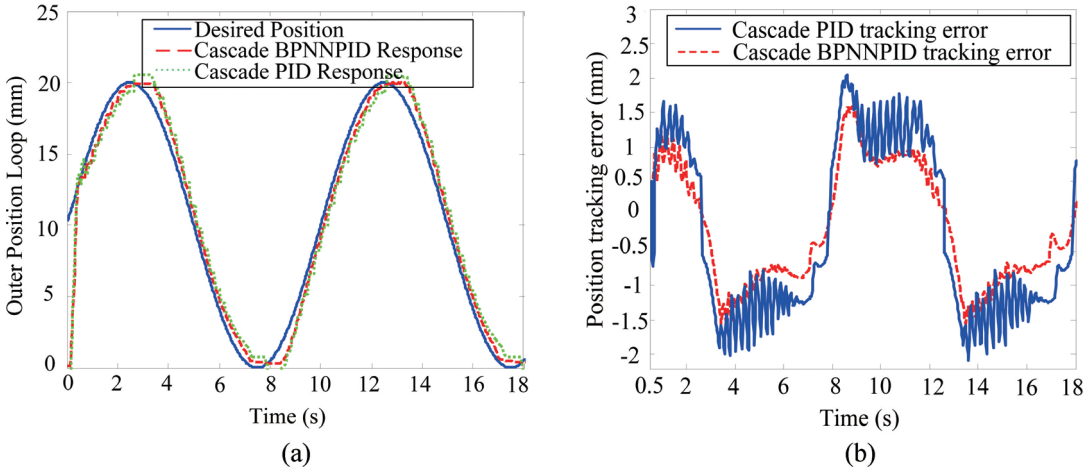

Fig. 9. Responses from the cascade BPNNPID scheme and conventional cascade PID scheme to sinusoid waves with 0.1 Hz and amplitude 20 mm: (a) Tracking responses; (b) Position tracking errors.

0.1 Hz with amplitude 20 mm are applied to PAM, and corresponding responses of BPNNPID controller and classic PID controller are plotted in Fig. 9(a). Position tracking error curves are plotted in Fig. 9(b), which indicate that BPNNPID controller has better capacity in precisely tracking position than classic PID controller.

5. Conclusion

In this research, a new cascade controller to realize accurate position controll is designed by incorporating BP Neural Network and PID algorithm. Polynomial model of PAM is identified using experimental data. Then a BPNN tuned PID controller is introduced. Experimental validations are performed.

Comparison between experimental curves of the designed BPNN tuned PID scheme and curves of conventional PID scheme demonstrates the better capacity of the proposed controller in position tracking. The effective performance of the adaptive controller inspires to use PAM in rehabilitation robots and devices.

Acknowledgments

This research was funded by National Natural Science Foundation of China (51005052); the Ministry of Education Doctoral Education Foundation (200802131005); Harbin Institute of Technology Research and Innovation Fund (HIT.NSRIF.2009016); State Key Laboratory of independent topics (SKLRS201001C).

References

[1] Chen Y, Li G, Zhu Y, Zhao J and Cai H. Design of a 6-DOF upper limb rehabilitation exoskeleton with parallel actuated joints. Bio-Medical Materials and Engineering. 2014; 24: 2527-2535.
[2] Leire L-S, Begonya G-Z and Amaia M-Z. Memory and accurate processing brain rehabilitation for the elderly: LEGO robot. Bio-Medical Materials and Engineering. 2014; 24: 3549-3556.
[3] Chang M-K. An adaptive self-organizing fuzzy sliding mode controller for a 2-DOF rehabilitation robot actuated by pneumatic muscle actuators. Control Engineering Practice. 2010; 18: 13-22.
[4] Xie SQ and Jamwal PK. An iterative fuzzy controller for pneumatic muscle driven rehabilitation robot. Expert Systems with Applications. 2011; 38: 8128-8137.
[5] Inoue K. Rubbertuators and applications for robots. In: Proceedings of the 4^{th} Symposium on Robotics Research, Tokyo. 1987; p. 57-63.
[6] Caldwell DG, Medrano-Cerda GA and Goodwin M. Control of pneumatic muscle actuators. IEEE Control Syst Mag. 1995; 15: 40-48.
[7] Chou C and Hannaford B. Measurement and modeling of McKibben pneumatic artificial muscles. IEEE Transactions on Robotica and Automation. 1996; 12(1): 90-102.
[8] Tsagarakis N and Caldwell DG. Improved modeling and assessment of pneumatic muscle actuators. In: Proceedings of the IEEE International Conference on Robotics & Automations, San Francisco. April 2000; p. 3641-3646.
[9] Glenn KK and Blake H. Accounting for elastic energy storage in McKibben artificial muscle actuators. Transactions of ASME, Journal of Dynamic Systems, Measurement and Control. 2000; 122: 386-388.
[10] Bertetto AM and Ruggiu M. Characterization and modeling of air muscles. Mechanics Research Communications. 2004; 31: 185-194.
[11] Deepak T, Amir L and Christopher DR. Geometrically exact models for soft robotic manipulators. IEEE Transactions on Robotics. 2008; 24(4): 773-780.
[12] Tondu B and Lopez P. Modeling and control of McKibben artificial muscle robot actuators. IEEE Control Systems Magazine. April 2000; 20(2): 15-38.
[13] Davis S and Darwin GC. Braid effects on contractile range and friction modeling in pneumatic muscle actuators. The International Journal of Robotics Research. 2006; 25(4): 359-369.
[14] Van DM, Beyl P, Vanderborght B, Van HR, Vanderniepen I, Versluys R et al. Modeling hysteresis in pleated pneumatic artificial muscles. In: Proceedings of IEEE Conference on Robotics, Automation and Mechatronics. 2008; p. 471-476.
[15] Tri VM, Tegoeh T, Herman R and Hendrik VB. Cascade position control of a single pneumatic artificial muscle-mass system with hysteresis compensation. Mechatronics. 2010; 20: 402-414.
[16] Caldwell DG, Medrano-Cerda GA and Goodwin MJ. Control of pneumatic muscle actuators. IEEE Control Systems Magazine. 1995; 15(1): 40-48.
[17] Repperger DW, Phillips CA and Krier M. Controller design involving gain scheduling for a large scale pneumatic muscle actuator. In: Proceedings of IEEE International Conference on Control Applications. 1999; p. 285-290.
[18] Lilly JH and Yang L. Sliding mode tracking for pneumatic muscles actuators in opposing pair configuration. IEEE Trans Control System Technology. 2005; 13(4): 550-558.
[19] Chan SW, Lilly JH, Repperger DW and Berlin JE. Fuzzy PD+I learning control for a pneumatic muscle. In: IEEE International Conference on Fuzzy Systems. 2003; p. 278-83.

[20] Thanh TDC and Ahn KK. Nonlinear PID control to improve the control performance of 2 axes pneumatic artificial muscle manipulator using neural network. Mechatronics. 2006; 16: 577-587.
[21] Balasubramanian K and Rattan KS. Trajectory tracking control of a pneumatic muscle system using fuzzy logic. Fuzzy Information Processing Society, Annual Meeting of the North American. 2005; p. 472-477.
[22] Yin J-M, Shin J-S and Lee H-H. On-line tuning PID parameters in an idling engine based on a modified BP neural network by particle swarm optimization. Artif Life Robotics. 2009; 14: 129-133.